Available online at www.sciencedirect.com
ScienceDirect
Journal of Computational Physics 227 (2008) 4441–4458
JOURNAL OF COMPUTATIONAL PHYSICS
www.elsevier.com/locate/jcp

A direct simulation method for flows with suspended paramagnetic particles ☆

Tae Gon Kang, Martien A. Hulsen *, Jaap M.J. den Toonder, Patrick D. Anderson, Han E.H. Meijer

Materials Technology, Eindhoven University of Technology, P.O. Box 513, 5600 MB Eindhoven, The Netherlands

Received 21 February 2007; received in revised form 31 October 2007; accepted 3 January 2008
Available online 17 January 2008

Abstract

A direct numerical simulation method based on the Maxwell stress tensor and a fictitious domain method has been developed to solve flows with suspended paramagnetic particles. The numerical scheme enables us to take into account both hydrodynamic and magnetic interactions between particles in a fully coupled manner. Particles are assumed to be non-Brownian with negligible inertia. Rigid body motions of particles in 2D are described by a rigid-ring description implemented by Lagrange multipliers. The magnetic force, acting on the particles due to magnetic fields, is represented by the divergence of the Maxwell stress tensor, which acts as a body force added to the momentum balance equation. Focusing on two-dimensional problems, we solve a single-particle problem for verification. With the magnetic force working on the particle, the proper number of collocation points is found to be two points per element. The convergence with mesh refinement is verified by comparing results from regular mesh problems with those from a boundary-fitted mesh problem as references. We apply the developed method to two application problems: two-particle interaction in a uniform magnetic field and the motion of a magnetic chain in a rotating field, demonstrating the capability of the method to tackle general problems. In the motion of a magnetic chain, especially, the deformation pattern at break-up is similar to the experimentally observed one. The present formulation can be extended to three-dimensional and viscoelastic flow problems.

PACS: 02.70.Dh; 47.50.Gj; 47.61.−k; 83.80.Gv

Keywords: Magnetic particle; Maxwell stress tensor; Fictitious domain method; Finite element method; Rotating magnetic field

1. Introduction

There are many areas that involve active manipulation of suspensions of micron-sized magnetic particles. Magneto-rheological (MR) fluids consist of magnetizable particles suspended in a non-magnetic medium.

☆ Supplementary movies for Figs. 11 and 14 are available at http://www.mate.tue.nl/~hulsen/magnetic/magnetic.zip.

* Corresponding author. Tel.: +31 40 247 5081; fax: +31 40 244 7355.
E-mail address: m.a.hulsen@tue.nl (M.A. Hulsen).

0021-9991/$ - see front matter © 2008 Elsevier Inc. All rights reserved.
doi:10.1016/j.jcp.2008.01.005

Upon applying a magnetic field the particles align into chains or clusters so that the MR fluid exhibits rigid behavior with a yield stress. It is this field-dependent rheological structure formation and yield stress, combined with their rapid response to the application of a magnetic field, that makes MR fluids an attractive technology for a number of challenging applications [1,2]. Since the appearance of the concept of micro-total-analysis systems [3], recently, suspensions of paramagnetic particles are employed in a newly emerging field: microfluidics for chemical or bio-medical applications [4,5]. The magnetic manipulation of the particles provides an additional degree of freedom to the system compared with normal microfluidic or biological systems [4]. In these microfluidic systems, small magnetic particles are used as mobile substrates for bio-assays to be transported to the desired position [6,7] or as stirring agents in order to achieve enhanced mixing [8,9].

When exposed to an externally applied magnetic field, the magnetically polarizable particles acquire dipole moments and the induced moments interacting with each other lead to the formation of chain-like structures or clusters of particles aligned with the field direction [10–12]. The motion of an individual particle and the dynamics behind the formation of magneto-rheological structures (MRS) are key issues from a fundamental point of view. To date, many numerical studies have been reported to understand the dynamics of the particles influenced by magnetic fields. Most of them focus on the dynamics of the particles and the formation of magneto-rheological structures using a numerical method based on the Stokes drag law and the dipole–dipole interaction model, neglecting hydrodynamic interactions between particles and higher-order mutual magnetic interactions between closely spaced particles. Flow characteristics induced by the particle motion and the particle motion affected by the flow received less attention due to the lack of a proper numerical model to take into account both hydrodynamic and magnetic interactions in a fully coupled manner.

In this work, we introduce a direct numerical simulation scheme to fully couple both hydrodynamic and magnetic interactions in flows with suspended magnetic particles in an externally applied magnetic field. Particles are assumed to be non-Brownian and inertialess and fluid flow is governed by the Stokes equation neglecting inertia. We make use of a toolkit for the finite element method [13] as a base on which our numerical implementation is developed. The flow problem with rigid particles is solved using a fictitious domain [14] and the finite element method to take into account the hydrodynamic interactions. The forces working on the particles due to an external magnetic field and magnetic interactions between the particles are implemented through the Maxwell stress tensor formulation. In this formulation, the magnetic force, which is added as a body force to the momentum equations, is represented by the divergence of the Maxwell stress tensor [15,16] evaluated from the magnetic field intensity obtained as a solution of Maxwell's equations. The dipole moment method used by other authors is quite effective if the length scale of the field non-uniformity is much larger than the particle size [17,18]. However, this assumption may be violated in microfluidic applications because practical sources of magnetic fields, for example permanent magnets or current-carrying wires, become smaller with miniaturization, leading to the decrease in the length scale of the field non-uniformity as well. Therefore, in applications with the particle size comparable to the field non-uniformity due to closely spaced particles or particles close to a magnetic source, the present approach is more favorable than that based on the dipole moment method. From the viewpoint of implementation, moreover, the present scheme has several advantages: (1) easy implementation in a code based on the finite element method, regardless of the shape of particles; (2) easy treatment of inhomogeneous magnetic permeability, possibly also depending on the magnetic field intensity; and (3) direct simulation of particulate flows with both hydrodynamic and magnetic interactions.

We focus on simulations of two-dimensional circular particles suspended in a non-magnetic Newtonian fluid in order to introduce the numerical scheme and study its feasibility for extension to much more computationally intensive three-dimensional problems. The present paper is organized as follows. We first introduce the problem we wish to solve. Next we address the essence of the finite element formulations for the governing equations: Maxwell's equations and Stokes equations. Then we show the validity of our formulation using a single-particle problem. Finally we solve two example problems involving magnetic particles subjected to either a uniform or a rotating magnetic field, as applications to demonstrate the capability of our numerical scheme.

2. Modeling

2.1. Problem definition

The problem we wish to solve is, as schematically illustrated in Fig. 1, the motion of paramagnetic particles and fluid flow in an externally applied magnetic field taking into account both hydrodynamic and magnetic interactions in a fully coupled manner. Paramagnetic particles are magnetically neutral in the absence of a magnetic field, but magnetized under the influence of an external magnetic field. We neglect the effect of magnetic saturation, which is an approximation for relatively small field strengths. The particles are assumed to be non-Brownian and inertialess, but they interact with the surrounding fluid and other particles both hydrodynamically and magnetically. The constant magnetic permeabilities of the particles and the fluid are μ_p and μ_0, respectively, where $\mu_p > \mu_0$. The magnetic permeability of the non-magnetic fluid is the same as that in vacuum. Here we assume that the magnetic field is generated by static current (or very slowly changing current) so that we may solve magnetostatics which is a special case of Maxwell's equations in the absence of an electric field and electrostatic charges [15,19]. The fluid is Newtonian with the viscosity η. The fluid flow is assumed to be governed by the viscous force and the magnetic actuation acting on the particles, neglecting the effect of inertia.

A typical computational domain consists of particles all with the same radius a suspended in a cavity filled with a non-magnetic Newtonian fluid. We impose a magnetic flux density $\boldsymbol{B}_0$ applied externally as an essential boundary condition at the cavity boundary, which will be discussed in the next section. Here the magnetic flux density at the cavity boundary is the only driving force to actuate the particles and thereby induce fluid flow. Particles are denoted by $P_i(t)$ $(i = 1, \ldots, N)$, where N is the number of particles in the cavity. We define $P(t) = \bigcup_{i=1}^{N} P_i(t)$ as a collective region occupied by the particles at time t. The fluid domain is denoted by $\Omega \setminus P(t)$ at time t with Ω being the entire region. In the following sections, the governing equations and boundary conditions for both magnetic and flow problems will be discussed in detail.

2.2. Magnetostatic problem

2.2.1. Governing equations

The problem of electromagnetic analysis is actually a problem of solving a set of Maxwell's equations subjected to given boundary conditions [19]. In the case of a magnetostatic field, the governing equations can be written as

$$\nabla \times \boldsymbol{H} = \boldsymbol{J}, \tag{1}$$

$$\nabla \cdot \boldsymbol{B} = 0, \tag{2}$$

where $\boldsymbol{H}$ is the magnetic field intensity, $\boldsymbol{J}$ the current density, and $\boldsymbol{B}$ the magnetic flux density. In order to solve the two Maxwell's equations for magnetostatics, we need a constitutive equation relating the two field quantities, $\boldsymbol{B}$ and $\boldsymbol{H}$. The constitutive equation describing macroscopic properties of the medium being considered is

$$\boldsymbol{B} = \mu \boldsymbol{H}, \tag{3}$$

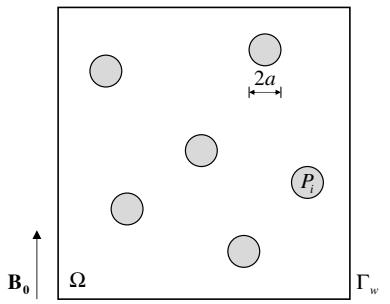

Fig. 1. Magnetic particles with the permeability μ_p suspended in a non-magnetic fluid with the permeability μ_0 under the influence of an externally applied magnetic field. The surrounding medium is a Newtonian fluid with the viscosity η. Here $\boldsymbol{B}_0$ is the magnetic flux density applied externally.

where μ denotes the magnetic permeability of a linear isotropic medium. In general, to solve the magnetostatic Maxwell's equations, the first-order partial differential equations are converted into second-order partial differential equations involving only one field variable called the magnetic vector potential $\boldsymbol{A}$. The magnetic flux density can be represented by the curl of $\boldsymbol{A}$,

$$\boldsymbol{B} = \nabla \times \boldsymbol{A}, \tag{4}$$

which satisfies Eq. (2). Thus, the magnetostatic field governed by Eqs. (1) and (2) may be represented by the second-order partial differential equations,

$$\nabla \times \left(\frac{1}{\mu}\nabla \times \boldsymbol{A}\right) = \boldsymbol{J}. \tag{5}$$

To uniquely define the vector potential, in addition to Eq. (5), a gauge condition for $\boldsymbol{A}$ is required [19]. The particular choice used in this study is Coulomb gauge, given by $\nabla \cdot \boldsymbol{A} = 0$.

The magnetic permeability μ, which is discontinuous at fluid–particle interfaces, is evaluated by the following equations, which is similar to the interpolation of material properties in the level set method [20],

$$\mu(\phi) = \begin{cases} \mu_{\mathrm{p}} & \text{if } \phi \leqslant 0 \text{ (particle domain)}, \\ \mu_0 & \text{otherwise (fluid domain)}, \end{cases} \tag{6}$$

where ϕ is the signed distance function from a spatial position $\boldsymbol{x}$ to the particle boundaries $\partial P_i(t)$ defined by

$$\phi(\boldsymbol{x}) = \min\{|\boldsymbol{x} - \boldsymbol{X_i}| - R_i\} \quad (i = 1, \cdots, N), \tag{7}$$

where $\boldsymbol{X_i}$ is the position vector of the center of the ith particle, R_i the radius of the ith particle, and N the number of particles.

For two-dimensional cases, assuming a vertical current, $\boldsymbol{J} = J\boldsymbol{e}_z$, that is independent of the coordinate z, the magnetic vector potential has only a z-component, i.e. $\boldsymbol{A} = (0, 0, A)$, which satisfies the vector potential equation

$$\nabla \times \left(\frac{1}{\mu_{\mathrm{r}}}\nabla \times A\boldsymbol{e}_z\right) = \mu_0 J\boldsymbol{e}_z, \tag{8}$$

where μ_{r} is the relative permeability, $\mu_{\mathrm{r}} = \mu/\mu_0$, with μ_0 being the permeability in vacuum. In the Cartesian coordinate system, the z-component of above equation becomes

$$-\frac{\partial}{\partial x}\left(\frac{1}{\mu_{\mathrm{r}}}\frac{\partial A}{\partial x}\right) - \frac{\partial}{\partial y}\left(\frac{1}{\mu_{\mathrm{r}}}\frac{\partial A}{\partial y}\right) = \mu_0 J, \tag{9}$$

which has exactly the same form as a scalar diffusion equation with the diffusivity $1/\mu_{\mathrm{r}}$ and the source term $\mu_0 J$. Eq. (9) can be easily solved by the standard finite element method. Note that, since A is defined on xy-plane, i.e. $A = A(x, y)$, Coulomb gauge condition, $\nabla \cdot \boldsymbol{A} = 0$, is automatically satisfied.

Once the magnetic potential A is found, the components of the magnetic flux density, $\boldsymbol{B} = (B_x, B_y)$, are computed by

$$B_x = \frac{\partial A}{\partial y}, \quad B_y = -\frac{\partial A}{\partial x}. \tag{10}$$

2.2.2. Continuity conditions at the interface

At a current-free interface between two media, for example a fluid–particle interface having different magnetic permeabilities, the fields should satisfy two continuity equations, given by

$$\boldsymbol{n} \cdot (\boldsymbol{B}_{\mathrm{f}} - \boldsymbol{B}_{\mathrm{p}}) = 0, \tag{11}$$

$$\boldsymbol{n} \times (\boldsymbol{H}_{\mathrm{f}} - \boldsymbol{H}_{\mathrm{p}}) = 0, \tag{12}$$

where $\boldsymbol{n}$ is the unit vector normal to the interface pointing from the particle domain to the fluid. The two equations represent the continuity of the normal component of $\boldsymbol{B}$ and the tangential component of $\boldsymbol{H}$ at the interface. In Eqs. (11) and (12), the variables with the subscript 'f' and 'p' represent those variables evaluated from

the fluid domain and the particle domain, respectively. In terms of the magnetic potential A, the continuity conditions are given by

$$A_{\mathrm{f}} = A_{\mathrm{p}}, \tag{13}$$

$$\frac{1}{\mu_{\mathrm{r_f}}}\frac{\partial A_{\mathrm{f}}}{\partial n} = \frac{1}{\mu_{\mathrm{r_p}}}\frac{\partial A_{\mathrm{p}}}{\partial n}, \tag{14}$$

where $\frac{\partial}{\partial n} = \boldsymbol{n}\cdot\nabla$. In Section 2.2.5, we will show that the continuity equations, Eqs. (13) and (14), satisfy the original continuity equations, Eqs. (11) and (12).

2.2.3. Boundary conditions

As already mentioned, the magnetic flux density is given at a cavity boundary as an essential boundary condition. Therefore, the values of the magnetic potential A may be explicitly defined at the boundary via a Dirichlet boundary condition. In the two-dimensional Cartesian coordinate system, the form of A at the boundary is specified by the parameters A_0, A_1, and A_2 as follows:

$$A = A_0 + A_1 x + A_2 y, \tag{15}$$

where A_0 is an arbitrary constant (here defined to be zero, $A_0 = 0$). From Eq. (10), the two coefficients, A_1 and A_2, are given by $A_1 = -B_{0y}$ and $A_2 = B_{0x}$ for the prescribed external flux density $\boldsymbol{B}_0 = (B_{0x}, B_{0y})$.

2.2.4. Maxwell stress tensor

In order to describe the particle motion and the flow influenced by a magnetic field, one needs to have a relation between the magnetic field and the force acting on the particles due to the field. We employ the Maxwell stress tensor for this purpose. The Maxwell stress tensor $\boldsymbol{T}_{\mathrm{m}}$ due to the magnetic field is defined by

$$\boldsymbol{T}_{\mathrm{m}} = \mu\left(\boldsymbol{H}\boldsymbol{H} - \frac{1}{2}H^2\boldsymbol{I}\right), \tag{16}$$

where $\boldsymbol{I}$ is the identity tensor and $H^2 = \boldsymbol{H}\cdot\boldsymbol{H}$. The body force $\boldsymbol{f}_{\mathrm{m}}$ experienced by materials in the magnetic field is given by the divergence of $\boldsymbol{T}_{\mathrm{m}}$, $\boldsymbol{f}_{\mathrm{m}} = \nabla\cdot\boldsymbol{T}_{\mathrm{m}}$ [15]. The force $\boldsymbol{f}_{\mathrm{m}}$ may be regarded as a force density per volume (per area in 2D) exerted on the material body in the presence of the magnetic field, which contributes to the momentum balance equation as an external force. For example, the momentum balance equation under the influence of the magnetic field is represented by

$$\rho\left(\frac{\partial \boldsymbol{u}}{\partial t} + \boldsymbol{u}\cdot\nabla\boldsymbol{u}\right) = \nabla\cdot\boldsymbol{\sigma} + \nabla\cdot\boldsymbol{T}_{\mathrm{m}}, \tag{17}$$

where ρ denotes the density, $\boldsymbol{u}$ the velocity vector, t the time, and $\boldsymbol{\sigma}$ the Cauchy stress tensor.

2.2.5. Remarks

(1) The derivatives $\frac{\partial A}{\partial s}$ and $\frac{1}{\mu}\frac{\partial A}{\partial s}$ at the boundary can be introduced as follows:

$$\begin{aligned}\frac{\partial A}{\partial s} = \boldsymbol{s}\cdot\nabla A &= s_x\frac{\partial A}{\partial x} + s_y\frac{\partial A}{\partial y}\\ &= (-n_y)(-B_y) + n_x B_x \quad (s_x = -n_y, s_y = n_x)\\ &= \boldsymbol{B}\cdot\boldsymbol{n} \quad \text{(continuous at the interface)},\end{aligned} \tag{18}$$

$$\frac{1}{\mu}\frac{\partial A}{\partial s} = \boldsymbol{H}\cdot\boldsymbol{n} \quad \text{(discontinuous at the interface)}, \tag{19}$$

where $\boldsymbol{n}$ and $\boldsymbol{s}$ are the unit outward normal vector and the unit tangential vector at the interface, respectively. Therefore, $\frac{\partial A}{\partial s}$ and $\frac{1}{\mu}\frac{\partial A}{\partial s}$ are the normal components of $\boldsymbol{B}$ and $\boldsymbol{H}$ at the interface, respectively. From Eqs. (13) and (18), $\boldsymbol{B}\cdot\boldsymbol{n}$ is continuous at the boundary, which proves that Eq. (11) is fulfilled.

(2) The derivatives $\frac{\partial A}{\partial n}$ and $\frac{1}{\mu}\frac{\partial A}{\partial n}$ at the boundary can be introduced as follows:

$$\begin{aligned}\frac{\partial A}{\partial n} &= \boldsymbol{n}\cdot\nabla A = n_x\frac{\partial A}{\partial x} + n_y\frac{\partial A}{\partial y}\\ &= s_y(-B_y) - s_xB_x\\ &= -\boldsymbol{B}\cdot\boldsymbol{s} \quad \text{(discontinuous at the interface)},\end{aligned} \tag{20}$$

$$\frac{1}{\mu}\frac{\partial A}{\partial n} = -\boldsymbol{H}\cdot\boldsymbol{s} \quad \text{(continuous at the interface)}. \tag{21}$$

Therefore, $\frac{\partial A}{\partial n}$ and $\frac{1}{\mu}\frac{\partial A}{\partial n}$ are the tangential components of $\boldsymbol{B}$ and $\boldsymbol{H}$ at the interface with negative signs, respectively. From Eqs. (14) and (21), $\boldsymbol{H}\cdot\boldsymbol{s}$ is continuous at the interface, thus Eq. (12) holds.

(3) The continuity of the tangential component of $\boldsymbol{H}$, which is represented by the continuity of flux in the diffusion equation of the magnetic potential A, Eq. (14), is weakly satisfied in the finite element formulation.

(4) Note that, for linear isotropic homogeneous materials, the magnetic force $\boldsymbol{f}_{\mathrm{m}}$ is represented by [16]

$$\boldsymbol{f}_{\mathrm{m}} = \nabla\cdot\boldsymbol{T}_{\mathrm{m}} = \boldsymbol{J}\times\boldsymbol{B} - \frac{H^2}{2}\nabla\mu. \tag{22}$$

Therefore, without a free current density $\boldsymbol{J}$, the magnetic force $\boldsymbol{f}_{\mathrm{m}}$ acting on a medium with a constant magnetic permeability μ is zero. The forcing on a particle will therefore be singular due to the jump in the value of μ and will only act at the boundary of the particle.

2.3. Flow problem

2.3.1. Governing equations

We assume that the fluid flow is governed by the Stokes equations and the two-dimensional circular particles are assumed to be force-free, torque-free, and inertialess. The set of equations describing fluid flow in $\Omega\setminus P(t)$ is given by

$$-\nabla\cdot\boldsymbol{\sigma} = \nabla\cdot\boldsymbol{T}_{\mathrm{m}} \quad \text{in } \Omega\setminus P(t), \tag{23}$$

$$\nabla\cdot\boldsymbol{u} = 0 \quad \text{in } \Omega\setminus P(t), \tag{24}$$

$$\boldsymbol{\sigma} = -p\boldsymbol{I} + 2\eta\boldsymbol{D} \quad \text{in } \Omega\setminus P(t), \tag{25}$$

$$\boldsymbol{u} = \boldsymbol{U}_i + \boldsymbol{\omega}_i\times(\boldsymbol{x}-\boldsymbol{X}_i) \quad \text{on } \partial P_i(t)\ \ (i=1,\ldots,N), \tag{26}$$

$$\boldsymbol{u} = \boldsymbol{0} \quad \text{on } \Gamma_w, \tag{27}$$

where $\boldsymbol{\sigma}$ is the Cauchy stress tensor, $\boldsymbol{T}_{\mathrm{m}}$ the Maxwell stress tensor, $\boldsymbol{u}$ the velocity, p the pressure, η the viscosity, $\boldsymbol{D}$ the rate-of-deformation tensor, $\boldsymbol{U}_i$ the translational velocity of the ith particle, $\boldsymbol{\omega}_i$ the angular velocity of the ith particle, $\boldsymbol{x}$ the position vector of a point on the ith particle boundary, and $\boldsymbol{X}_i$ the position vector of the center of the ith particle. Eqs. (23)–(25) are the momentum balance equation, the continuity equation and the constitutive relation for the fluid domain, respectively. Eqs. (26) and (27) are the constraints for rigid body motion of the particles and the essential boundary condition at the solid wall to solve the set of governing equations, respectively.

As for the particle domain $P(t)$, we employ the rigid-ring description of Hwang et al. [21] where the fluid also fills the particles and the rigid body motion is imposed on the particle boundaries only. This description enables us to solve the same governing equations for both (fluid and particle) domains, reducing the number of unknowns for the rigid body constraints. The governing equations for a particle domain $P_i(t)$ at time t are the same as Eqs. (23)–(26) for the fluid domain. The trivial solution for the particle domain is the rigid body motion extended to the whole particle domain, $\boldsymbol{u} = \boldsymbol{U}_i + \boldsymbol{\omega}_i\times(\boldsymbol{x}-\boldsymbol{X}_i)$. Note that, the rigid-ring description is valid when inertia is negligible. If we solve a problem with inertia, rigid body constraints should be imposed inside the particle domain as well.

In addition to the above mentioned governing balance equations, boundary conditions, and constraints, one needs to solve the kinematic equations for the evolution of particle positions with time t, represented by

$$\frac{\mathrm{d}\boldsymbol{X}_i}{\mathrm{d}t} = \boldsymbol{U}_i, \quad \boldsymbol{X}_i(0) = \boldsymbol{X}_{i,0}. \tag{28}$$

Balance equations are needed for drag force and torque on particle boundaries in order to determine the unknown rigid body motions $(\boldsymbol{U}_i, \boldsymbol{\omega}_i)$ of the particles. In the absence of inertia,

$$\boldsymbol{F}_i = \int_{\partial P_i^+(t)} (\boldsymbol{\sigma} + \boldsymbol{T}_\mathrm{m}) \cdot \boldsymbol{n} \,\mathrm{d}S = 0, \tag{29}$$

$$\boldsymbol{T}_i = \int_{\partial P_i^+(t)} (\boldsymbol{x} - \boldsymbol{X}_i) \times ((\boldsymbol{\sigma} + \boldsymbol{T}_\mathrm{m}) \cdot \boldsymbol{n}) \,\mathrm{d}S = 0, \tag{30}$$

where $\boldsymbol{F}_i$ is the sum of the hydrodynamic drag and magnetic force, $\boldsymbol{T}_i$ the sum of the hydrodynamic torque and magnetic torque working on a rigid particle, and $\boldsymbol{n}$ is the outward normal vector at the particle boundary.

3. Finite element formulation

3.1. Magnetostatic problem

The weak form for the Poisson equation (9) for the magnetic potential A is given as: find $A \in \mathbb{S}$ such that

$$\int_\Omega \frac{1}{\mu_\mathrm{r}} (\nabla A \cdot \nabla \psi) \,\mathrm{d}A = \int_\Omega \mu_0 J \,\mathrm{d}A, \tag{31}$$

for all $\psi \in \mathbb{S}_0$ with $\mathbb{S} = \{A \in H^1(\Omega) \text{ with } A = \bar{A} \text{ at } \Gamma_w\}$ and $\mathbb{S}_0 = \{\psi \in H^1(\Omega) \text{ with } \psi = 0 \text{ at } \Gamma_w\}$. The weak form is used to obtain an approximate solution using the Galerkin finite element method. We used bi-quadratic interpolation for the magnetic potential A. The resulting matrix equation is solved using HSL/MA57, a sparse multi-frontal Gauss elimination method to solve a symmetric matrix [22].

3.2. Flow problem

The fluid flow problem, including interactions between fluid and rigid particles, is solved by using the finite element method and a fictitious domain method, similarly to previous work [21]. We use a fictitious domain method to treat rigid body constraints on particle boundaries. In the derivation of the weak form, following the approach of Glowinski et al. [14], fluid–particle interactions are implicitly treated through the combined weak formulation where hydrodynamic force and torque on the particle boundaries are canceled exactly. Since one can find the detailed derivation procedure in the existing literature [14,21] we present only the final weak form without detailed derivations. In the combined weak formulation, the rigid body constraint is enforced by the constraint equation using a Lagrange multiplier, $\boldsymbol{\lambda}^{p,i}$, defined on the particle boundary ∂P_i.

Let us first define the combined velocity and variational space for velocity, which is denoted by $\mathbb{V}$:

$$\begin{aligned} &\mathbb{V} = \{(\boldsymbol{u}, \boldsymbol{U}_i, \boldsymbol{\omega}_i) | \boldsymbol{u} \in H^1(\Omega)^2, \boldsymbol{U}_i \in \mathbf{R}^2, \boldsymbol{\omega}_i \in \mathbf{R}, \\ &\boldsymbol{u} = \boldsymbol{U}_i + \boldsymbol{\omega}_i \times (\boldsymbol{x} - \boldsymbol{X}_i) \text{ on } \partial P_i(t) \text{ and } \boldsymbol{u} = 0 \text{ on } \Gamma_w\} \end{aligned} \tag{32}$$

for $i = 1, \ldots, N$. For a given particle configuration $\boldsymbol{X}_i$ $(i = 1, \ldots, N)$, the weak form for the entire domain Ω can be stated as follows: find $(\boldsymbol{u}, \boldsymbol{U}_i, \boldsymbol{\omega}_i) \in \mathbb{V}$, $p \in \mathbf{L}^2(\Omega)$, and $\boldsymbol{\lambda}^{p,i} \in \mathbf{L}^2(\partial P_i(t))(i = 1, \ldots, N)$ such that

$$\begin{aligned} &\int_\Omega 2\eta \boldsymbol{D}(\boldsymbol{u}) : \boldsymbol{D}(\boldsymbol{v}) \,\mathrm{d}A - \int_\Omega p \nabla \cdot \boldsymbol{v} \,\mathrm{d}A \\ &\quad + \sum_{i=1}^{N} \langle \boldsymbol{\lambda}^{p,i}, \boldsymbol{v} - (\boldsymbol{V}_i + \boldsymbol{\chi}_i \times (\boldsymbol{x} - \boldsymbol{X}_i)) \rangle_{\partial P_i} = -\int_\Omega \boldsymbol{T}_\mathrm{m} : \boldsymbol{D}(\boldsymbol{v}) \,\mathrm{d}A, \end{aligned} \tag{33}$$

$$\int_\Omega q \nabla \cdot \boldsymbol{u} \,\mathrm{d}A = 0, \tag{34}$$

$$\langle \boldsymbol{\mu}^{p,i}(\boldsymbol{x}), \boldsymbol{u}(\boldsymbol{x}) - (\boldsymbol{U}_i + \boldsymbol{\omega}_i \times (\boldsymbol{x} - \boldsymbol{X}_i)) \rangle_{\partial P_i} = 0 \quad (i = 1, \ldots, N), \tag{35}$$

for all $(\boldsymbol{v}, \boldsymbol{V}_i, \boldsymbol{\chi}_i) \in \mathbb{V}$, $q \in L^2(\Omega)$, and $\boldsymbol{\mu}^{p,i} \in L^2(\partial P_i(t))$ $(i = 1, \ldots, N)$. In the weak formulations, the variables, $\boldsymbol{v}$, $\boldsymbol{V}_i$, $\boldsymbol{\chi}_i$, and q, are variations for the velocity $\boldsymbol{u}$, the translational velocity of a particle $\boldsymbol{U}_i$, the angular velocity of a particle $\boldsymbol{\omega}_i$, and the pressure p, respectively. As already mentioned, the force due to the magnetic field is given by the divergence of the Maxwell stress tensor. In the weak formulation, however, instead of using the divergence of the Maxwell stress tensor as it is, we applied integration by part and the Gauss' theorem. Thus this term is represented by the double inner product of the Maxwell stress and the rate-of-deformation tensor (see the term in right-hand side of Eq. (33)). This form enables us to circumvent differentiation of the Maxwell stress tensor which is discontinuous at fluid–particle interfaces.

We use bi-quadratic interpolation for the velocity and bi-linear interpolation for the pressure, the so called Q_2/Q_1 element. As for the rigid body constraints, the weak form is approximated by point collocation [21]. The resulting matrix equation is solved by a sparse direct method, HSL/MA57 [22].

Particle positions are updated by integrating the evolution equations of particles, Eq. (28), using the rigid body motions of particles obtained as a part of the solution. We employ explicit time integration schemes: the explicit Euler method at the first time step and the second-order Adams-Bashforth method from the second time step onwards [21].

4. Verification

In this section we verify our numerical scheme using a single-particle problem. Since there is no analytic solution for the problem of a two-dimensional magnetic particle suspended in a fluid, we compare results obtained from a regular mesh problem with those from the corresponding boundary-fitted mesh problem as a reference. As will be discussed in this section, a boundary-fitted mesh results in a convergent solution with mesh refinement, satisfying discontinuities of the pressure and the magnetic field at the fluid–particle interface. However, the mesh must be updated with the change of particle positions, thus making it very difficult to apply to general problems.

4.1. Test problem

The single-particle problem chosen for verification is schematically illustrated in Fig. 2. We choose a square cavity of length L with the particle P_1 located at the center of the cavity that is influenced by the magnetic field generated by a current-carrying wire. In the absence of the particle, in the cylindrical coordinate system with its origin at the center of the wire, only the circumferential component of the magnetic flux density $\boldsymbol{B}$ is non-zero, i.e., $B_r = 0$ and $B_z = 0$. From the Biot-Savart law, the circumferential component B_θ is represented as follows [15]:

$$B_\theta = \frac{\mu I}{2\pi r}, \tag{36}$$

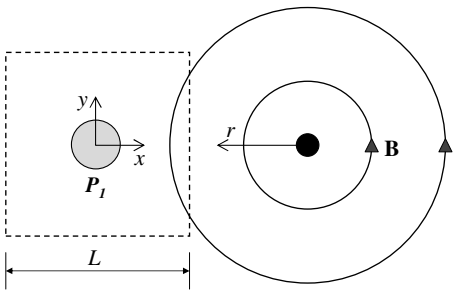

Fig. 2. Single-particle in a magnetic field generated by a current carrying wire. Given the current I and the magnetic permeability of the medium μ, the magnetic field around the wire is given by the Biot–Savart law.

where μ is the magnetic permeability of the medium, I the current passing through the wire, and r the radial distance from the wire to a certain spatial position. In this case, therefore, the magnetic potential A is a function of the radial coordinate r only, i.e., $A = A(r)$. Then the relation between B_θ and the magnetic potential A is given by

$$B_\theta = -\frac{\mathrm{d}A}{\mathrm{d}r}. \tag{37}$$

From Eqs. (36) and (37), therefore, the magnetic potential A around the wire is represented by

$$A = -\frac{\mu I}{2\pi}\ln r + A_0, \tag{38}$$

where A_0 is a constant set to be zero in this work. Eq. (38) is used to impose an essential boundary condition for A at the cavity boundary.

Just for verification of the method, we use in the simulations the following fixed material properties: viscosity η is 1, magnetic permeability of the fluid is 1 and of the particle is equal to 2, respectively. So the relative permeability of the particle μ_r is 2. The particle radius a is $a = 0.1L$ with the size of the cavity $L = 20$. In the boundary-fitted mesh problem, as depicted in Fig. 3(a), elements are generated such that the particle boundary coincides with internal boundaries of the elements. We use a discontinuous pressure element for the boundary fitted problem only. The collocation points are chosen to be nodal points on the particle boundary such that the rigid body constraint is satisfied at each node on the boundary. We performed mesh refinement to get a convergent solution for the problem. Shown in Table 1 is the translational velocity of the particle along x-direction, showing convergence with refinement of the boundary-fitted mesh. The results obtained from a boundary-fitted mesh, which is five-time finer than that shown in Fig. 3(a), are used as references. We use four regular meshes consisting of 34×34, 68×68, 102×102, and 136×136 elements, which are denoted by M1, M2, M3, and M4, respectively. Fig. 3(b) shows the mesh M1 with 42 collocation points.

4.2. Number of collocation points

We first investigate the effect of the number of collocation points (N_{cp}) at the particle boundary to determine the proper number of collocation points which guarantees the rigid body motion of the particle in the presence of magnetic actuation. We use mesh M3 (with 102×102 elements) varying the number of collocation points. Fig. 4 shows the relative error in the translational velocity of the particle U with refinement of collocation points. As reported in [21], one collocation point per element, where $N_{\mathrm{cp}} = 64$ in this specific example, seems to give the most accurate result in the sense of minimizing the error. In this plot we observe a plateau in the error around $N_{\mathrm{cp}} = 120$, above which the error begins to increase. Now let us examine the velocity field inside the particle domain. Plotted in Fig. 5 is the x-velocity u along the line ($y = 0$) to check if the rigid body motion inside the particle domain is guaranteed with one collocation point per element as well. As depicted in Fig. 5, however, the rigid body motion within the particle domain is not satisfied at all with $N_{\mathrm{cp}} = 64$, where overshoot and undershoot in velocity are observed and the velocity within the particle domain is not uniform. With refinement of collocation points, the velocity inside the particle becomes uniform and close to the reference solution obtained from the boundary-fitted mesh problem.

Thus, in the presence of magnetic actuation, one collocation point per element is not enough to satisfy the rigid body constraint inside the particle. As already mentioned, the body force $\boldsymbol{f}_m$ in a medium with a constant magnetic permeability is zero. Under the influence of magnetic fields, the body force is effective near the fluid–particle interface only, which is thought to be the reason that more collocation points per element are required than for problems with passive rigid particles without an actuation. From Figs. 4 and 5, two collocation points per element seems to be an optimal choice in the sense of minimizing the error in the rigid body motion of the particle and guaranteeing a uniform velocity inside the particle, allowing us to use the rigid-ring description in the problem with an actuation of the particle. As the number of collocation points increases to more than two points per element, the system becomes over-constrained, which results in an increased error in the solution. In simulations introduced hereafter, the number of collocation points per element is therefore equal to two.

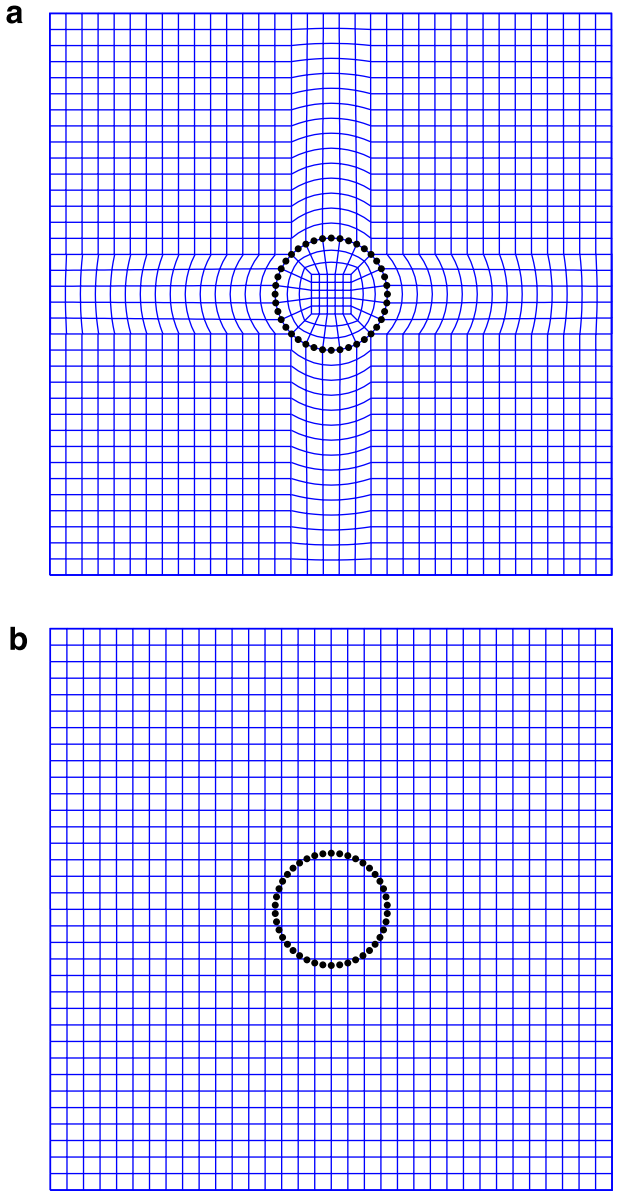

Fig. 3. Meshes for the problem of a single particle (represented by black dots) in a magnetic field generated by the current-carrying wire defined in Fig. 2. (a) A boundary-fitted mesh ($M_{bf}1$) and (b) a regular 34×34 mesh (M1). The coordinate of the particle center is (0, 0).

Table 1
Translational velocity U_{bf} of the particle (along x direction) with mesh refinement in boundary-fitted meshes

Mesh	Translational velocity of the particle, U_{bf}
$M_{bf}1$	1.5639866×10^{-2}
$M_{bf}2$	1.5640612×10^{-2}
$M_{bf}3$	1.5640662×10^{-2}
$M_{bf}4$	1.5640671×10^{-2}
$M_{bf}5$	1.5640674×10^{-2}

Here, $M_{bf}1$ represents a boundary-fitted mesh shown in Fig. 3(a), $M_{bf}2$ a refined mesh by two times, and so on.

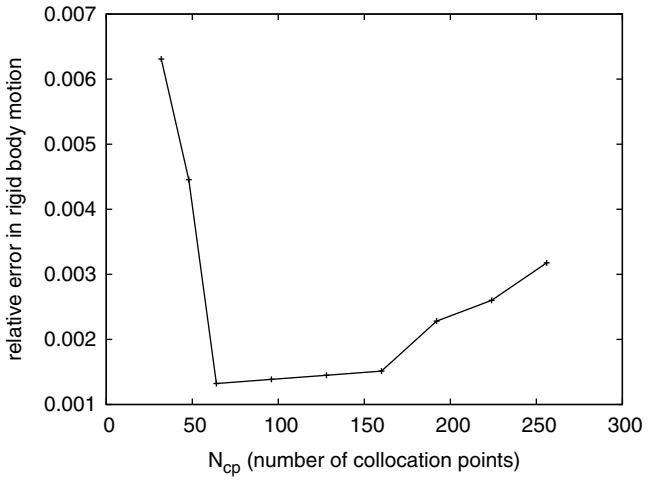

Fig. 4. Relative errors of the rigid body motion with the refinement of collocation points. Here only the translation velocity along x direction, U, is compared. The error is defined as $e = |\frac{U-U_{\mathrm{bf}}}{U_{\mathrm{bf}}}|$, where U_{bf} is the particle translational velocity obtained from the boundary-fitted mesh problem. The mesh used is M3. At the number of collocation points $N_{\mathrm{cp}} = 64$, there is one collocation point per element.

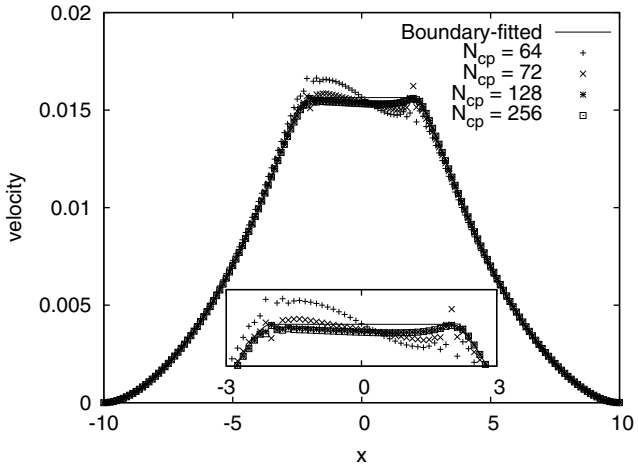

Fig. 5. Comparison of the x-velocity component u along the line $y = 0$ with the refinement of the number of collocation points, N_{cp}. The solid line is the velocity obtained from the boundary-fitted mesh problem and symbols from regular mesh problems with the mesh M3.

4.3. Convergence

Now we compare the magnetic flux density, the velocity, the pressure, and the shear rate obtained from the boundary-fitted mesh problem with those from regular mesh problems with mesh refinement.

Fig. 6 depicts the y component of the magnetic flux density B_y along the line $y = 0$. Since the tangential component of $\boldsymbol{B}$ is discontinuous at the fluid–particle interface, B_y is discontinuous at $x = \pm a$. Due to the discontinuity of permeability, we observe deviations from the reference solution at the coarse mesh M1, but the solution converges to the reference solution with mesh refinement. The x-velocity u along the line is plotted in Fig. 7. The coarse mesh M1 leads to an oscillatory velocity solution inside the particle with large overshoot and undershoot near the particle boundary. With mesh refinement, the velocity becomes uniform inside the particle and shows convergence to the result obtained from the boundary-fitted mesh. As plotted in Fig. 8, the pressure obtained with the coarse mesh M1 seems to be very poor near the particle boundary, where pressure is discontinuous across the boundary. Since the pressure inside the particle is undefined we compare the

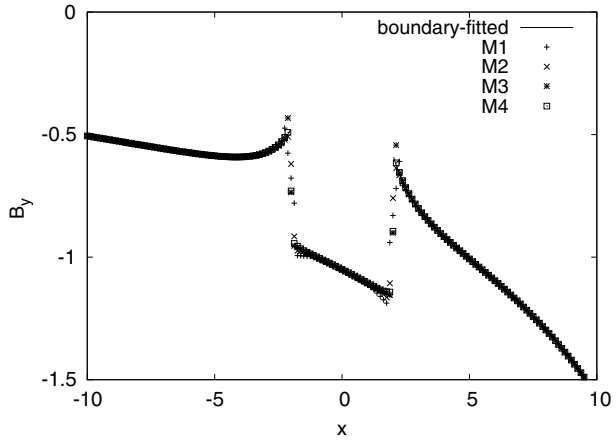

Fig. 6. Comparison of the y-component of the magnetic flux density B_y along the line $y = 0$ with mesh refinement. B_y is discontinuous at the fluid–particle interface.

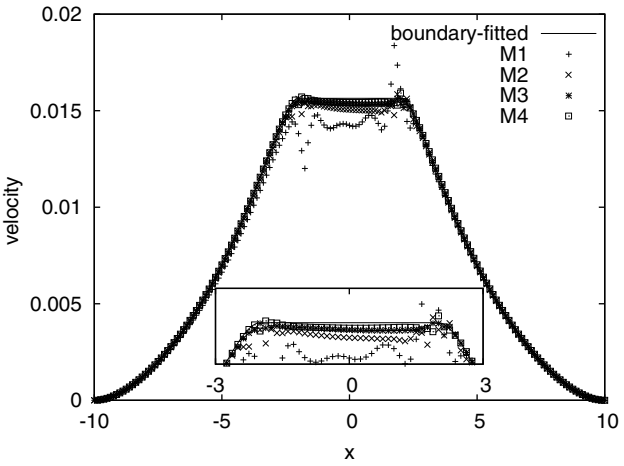

Fig. 7. Comparison of the x-velocity u along the line $y = 0$ with mesh refinement.

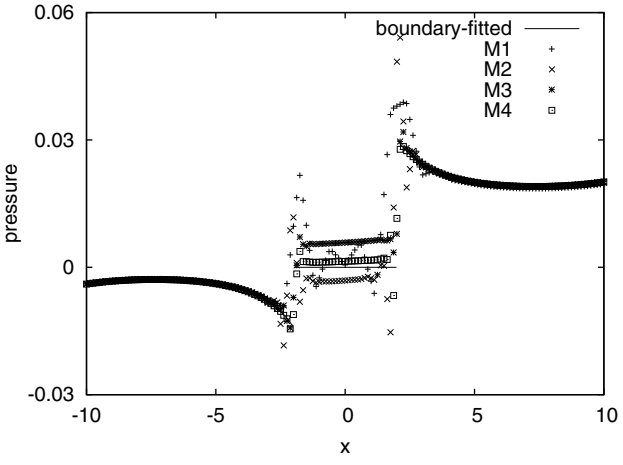

Fig. 8. Comparison of the pressure along the line $y = 0$ with mesh refinement.

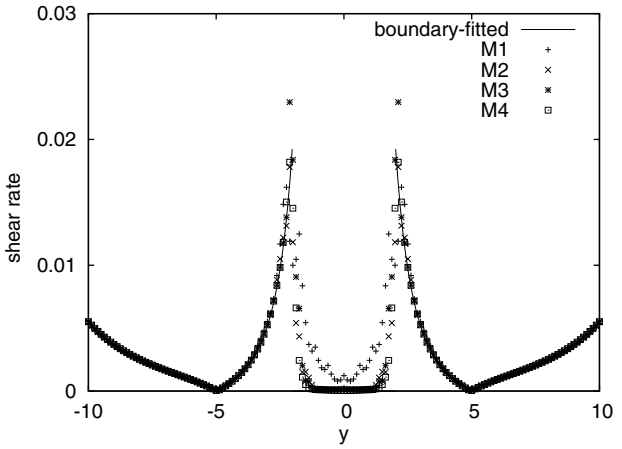

Fig. 9. Comparison of the generalized shear rate $\dot{\gamma}$ along the line $x = 0$ with mesh refinement. The generalized shear rate is defined as $\dot{\gamma} = \sqrt{2\boldsymbol{D} : \boldsymbol{D}}$, where $\boldsymbol{D} = \frac{1}{2}(\nabla \boldsymbol{u} + \nabla \boldsymbol{u}^{\mathrm{T}})$.

pressure in the fluid domain only and, with mesh refinement, the pressure here converges to the reference solution as well. Finally, we made a comparison for the generalized shear rate $\dot{\gamma}$, which in principle should be zero inside the particle. The generalized shear rate is defined as a square root of the second invariant of the rate-of-deformation tensor $\boldsymbol{D}$. The shear rate plotted along the line $x = 0$ looks good outside the particle domain even in the coarse meshes, see Fig. 9. In the coarse mesh M1, due to the oscillatory velocity solution inside the particle, the shear rate is not zero in the particle domain, but it shows convergence to zero shear rate with mesh refinement.

5. Applications

To demonstrate the capability of the method developed, we introduce results obtained from two problems with two and more circular magnetic particles of the same diameter $2a$ subjected to a uniform magnetic field and one rotating with an angular frequency ω.

5.1. Two magnetic particles in a uniform magnetic field

We first solve a problem consisting of two circular paramagnetic particles suspended in a fluid closed by a circular cavity of radius $R_c = 0.5$. The two particles are magnetically interacting with each other in a uniform magnetic field externally applied (see Fig. 10). The initial distance between the two centers of the particles is $4a$ with the particle radius $a = 0.05R_c$. Flow is induced only by the motion of the particles. The motion is caused

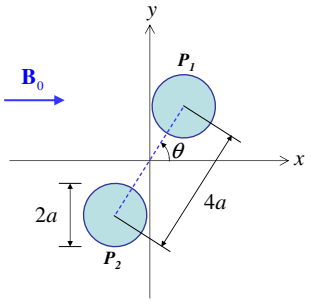

Fig. 10. Interaction of two magnetic particles in a uniform magnetic field directing horizontally. The angle θ is an angle formed by the magnetic field and the line connecting the two particles. The distance between the two particles is $4a$, where a is the radius of the particles

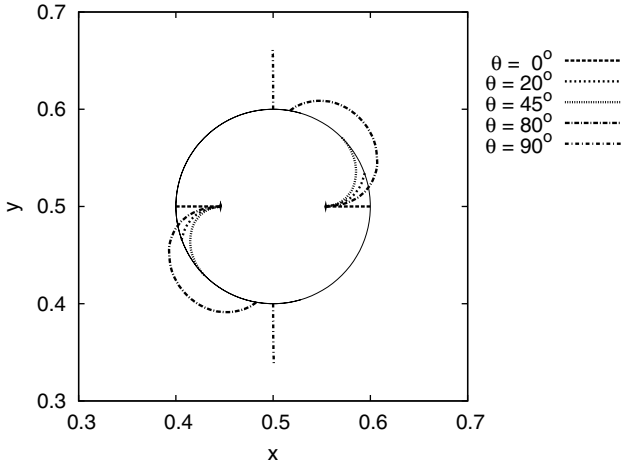

Fig. 11. Trajectories of the centers of the two particles in a uniform magnetic field at $\theta = 0°$, 20°, 45°, 80°, and 90°. The solid line is a circle of radius $4a$ where initial positions of the particles are located and other lines are trajectories of the particles influenced by the angle θ.

by the magnetic interactions between the particles due the externally applied field. The actual motion is dependent on the configuration of the particles.

It is well known that the force between two polarizable particles in a uniform magnetic field may be either attractive or repulsive depending on the angle θ formed between the direction of the applied field and the line connecting the two centers of the particles. In the case of spherical particles, an analytic formula for the force can be derived for the dipole–dipole interaction model [1]. The critical angle θ_c is 55° in the case of two spherical particles, i.e., the force is attractive at an angle less than θ_c and repulsive at an angle greater than θ_c.

In the case of two-dimensional circular particles, however, there is no analytical formula available. The cavity is discretized into 60,000 nine-node rectangular elements and the material parameters are the same as those used in the verification introduced in Section 4. Fig. 11 depicts trajectories of the particles showing different paths depending on the angle θ. From the simulations, we find that the critical angle θ_c in this case is approximately 45°. As shown in Fig. 11, in the end, the two particles are aligned with the applied field regardless of the initial angle θ, except for the case with $\theta = 90°$ at which the two particles moved away from each other. In reality, however, the two particles having a right angle with the field will also be aligned along the field direction due to any disturbance working on the particles, for example by Brownian motion of fluid particles colliding with the magnetic particles. Though we solve two-dimensional problems here, we show that our scheme can take into account magnetic interactions between the two particles coupled with hydrodynamic interactions.

5.2. Magnetic chain in a rotating magnetic field

The second problem is a two-dimensional circular cavity flow with particles (initially forming a chain aligned horizontally) suspended in a non-magnetic fluid in a rotating magnetic field. We here demonstrate the capability of our scheme to solve a problem involving such topological changes as break-up and reformation of the chain, significantly influenced by a non-dimensional number, the Mason number.

5.2.1. Scaling analysis

First of all, we wish to introduce the result of scaling analysis for the governing equations for the flow with magnetic particles, aiming to extract dimensionless parameters influencing the motion of fluid and particles. As introduced in Section 2.3, we solve a single governing equation for both fluid and particle domains with constraints for the rigid body motion. The fluid is assumed to be non-magnetic, so the magnetic permeability

of the fluid domain is μ_0. The particle is circular with radius a and is assumed to have a constant magnetic permeability μ_p which is larger than μ_0, i.e. $\mu_p > \mu_0$.

Non-dimensional variables (with a superscript *) are given by

$$x^* = \frac{x}{l_c}, \quad y^* = \frac{y}{l_c}, \tag{39}$$

$$\boldsymbol{u}^* = \frac{\boldsymbol{u}}{u_c}, \tag{40}$$

$$p^* = \frac{p}{p_c}, \tag{41}$$

$$T^*_{ij} = \frac{T_{ij} - \mu_0 H_c^2}{(\mu_p - \mu_0) H_c^2}, \tag{42}$$

where l_c denotes a characteristic length, $\boldsymbol{u}_c$ a characteristic velocity, p_c a characteristic pressure, and H_c the characteristic magnetic field intensity. Here we define the characteristic length, velocity and pressure as $l_c = a$, $u_c = a/t_c$ and $p_c = \eta u_c/a$, respectively. The Maxwell stress tensor is non-dimensionalized by the stress difference (with the reference being $\mu_0 H_c^2$) normalized by $(\mu_p - \mu_0)H_c^2$. The characteristic time scale t_c is defined as the inverse of the angular frequency ω. The magnetic flux density $\boldsymbol{B}_0$ has the form of

$$\boldsymbol{B}_0 = B_0(\cos(\omega t)\boldsymbol{e}_x + \sin(\omega t)\boldsymbol{e}_y). \tag{43}$$

The characteristic magnetic field intensity is defined as $H_c = H_0 = B_0/\mu_0$. Then, the resulting non-dimensional momentum equation for the Stokes flow is

$$\nabla^* p^* - \nabla^{*2}\boldsymbol{u}^* = \frac{1}{Ma}\nabla^* \cdot \boldsymbol{T}^*, \tag{44}$$

where Ma is the Mason number, which is the ratio of the viscous force to the magnetic force under the influence of a rotating magnetic field, defined by

$$Ma = \frac{\eta\omega}{\mu_0 \chi_p H_0^2}, \tag{45}$$

with χ_p being the magnetic susceptibility of the particle, defined by $\chi_p = \mu_p/\mu_0 - 1$. In Eq. (45), the Mason number may also be interpreted as the ratio of the time scale of magnetic particle motion, $t_m = \eta/(\mu_0\chi_p H_0^2)$, to the flow time scale t_c. The time scale t_m is related to the time required for a magnetic particle to travel the order of its size given the field intensity H_0 and surrounding fluid with the viscosity η. With all the other parameters, such as the ratio of particle size to cavity size a/R_c, the susceptibility χ_p, and the particle area fraction ϕ_a, being fixed, the Mason number is the only parameter influencing the dynamics of the chain and the flow in the cavity in a rotating magnetic field.

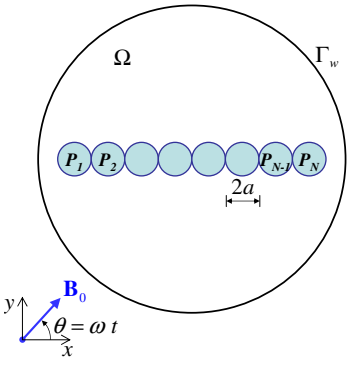

Fig. 12. Schematic representation of a magnetic chain in a circular cavity under the influence of a rotating magnetic field. A chain consisting of N magnetic particles is horizontally aligned initially.

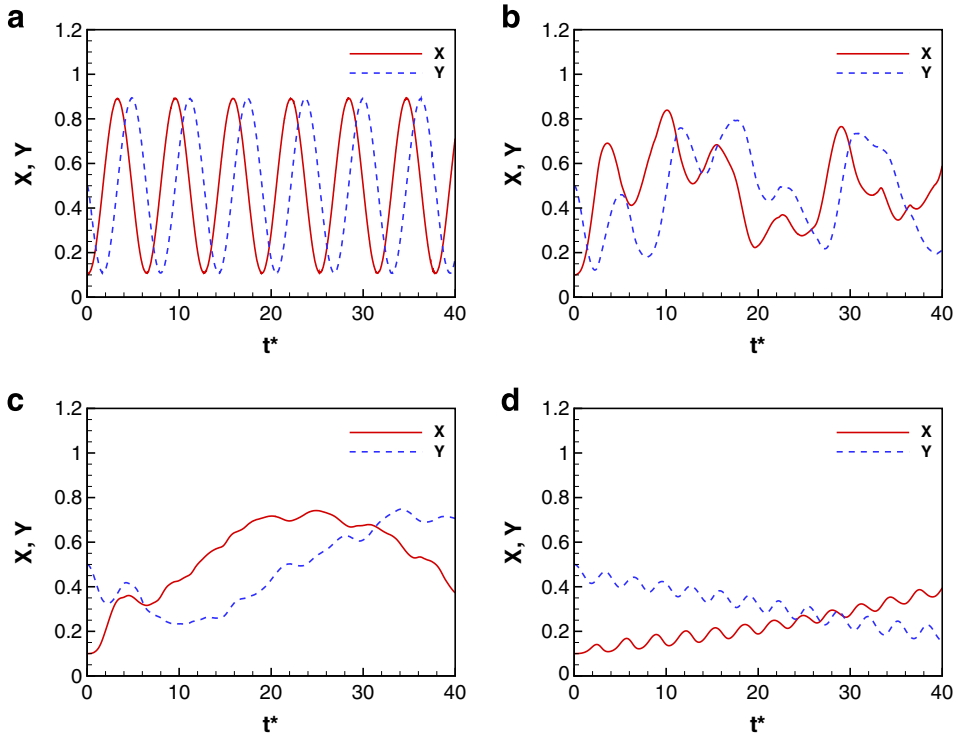

Fig. 13. Evolution of the particle position (X, Y) of the first particle at the four Mason numbers: (a) $Ma = 0.0005$; (b) $Ma = 0.002$; (c) $Ma = 0.005$; (d) $Ma = 0.01$. The abscissa is the non-dimensional time defined by $t^* = \omega t$. The initial location of the particle is (0.1, 0.5).

5.2.2. Chain motion and flow characteristics

We carry out simulations at four Mason numbers, $Ma = 0.0005$, 0.002, 0.005, and 0.01, attempting to investigate the dynamics of a magnetic chain and flow characteristics as significantly influenced by Mason numbers in this range. In the simulations, we fix the ratio of particle to cavity radius to be $a/R_c = 0.05$, so the area fraction of the particles equals $\phi_a = 0.0425$ when the number of particles $N = 17$ (see Fig. 12 for the definition of the particle). The cavity is discretized into 14,400 nine-node rectangular elements. The time step used is 0.02 in non-dimensional units. There are approximately eight elements along the particle diameter.

Fig. 13 plots the evolution of the particle position (X, Y) of the first particle P_1 initially located at (0.1, 0.5). As expected from the trajectory depicted in Fig. 13(a), at the low Mason number $Ma = 0.0005$ the chain rotates almost like a rigid chain following the rotating magnetic field of the angular frequency ω, but the chain lags behind the field. Chain break-up is observed at the two intermediate Mason numbers, $Ma = 0.002$ and 0.005. In the first case, the chain is splitted into two chains, recombining later to form a single chain again, which takes place in an alternating manner. The two flow portraits (see the streamlines depicted in Fig. 14) induced by the two alternating typical motions of the chain(s), which may be regarded as two stirrers, are thought to be a useful means for enhanced mixing [9], requiring further investigations. Deformation patterns shown in Fig. 14 clearly show the detailed shape of the chain at the moment of break-up and reformation. Especially the shape of the chain at break-up, which looks like a reversed S-like structure, is quite similar to the theoretical prediction based on the dipole–dipole interaction model and the experimentally observed one by Melle et al. [11,12]. In the second case, however, the chain is splitted into three chains, which remain as separate chains without joining together. At a higher Mason number, $Ma = 0.01$, the chain rotates counter-clock wise in overall sense, but with a oscillatory motion moving forward and backward. At an even higher Mason number, $Ma = 0.1$, we observe that the chain no longer follows the field and remains at its initial location with a small oscillatory motion.

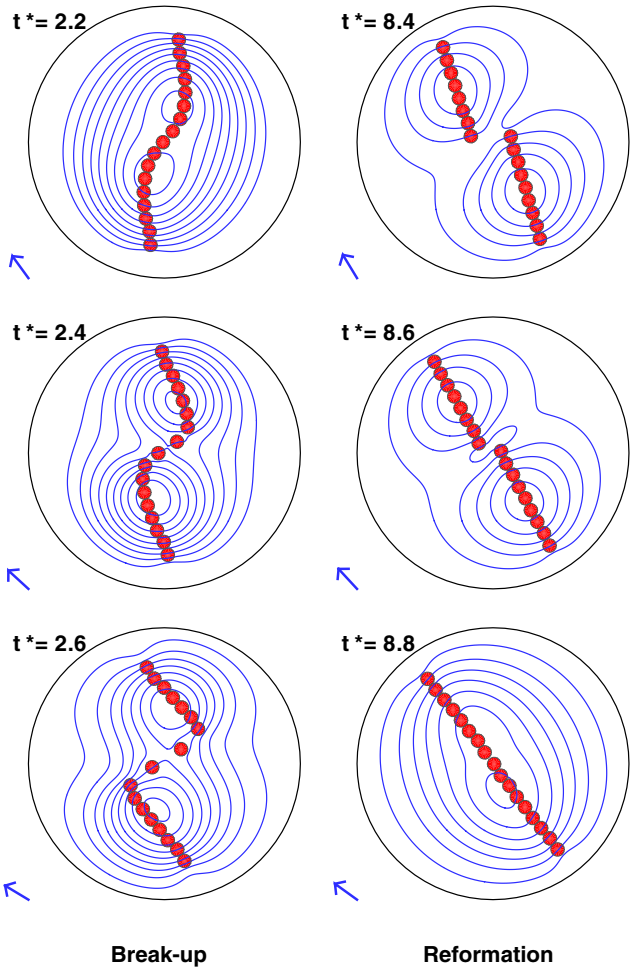

Fig. 14. Streamlines and chain configurations at the moment of chain break-up (left) and reformation (right) at $Ma = 0.002$. The arrow indicates the direction of the magnetic field at a non-dimensional time t^*.

6. Conclusion

A new direct numerical simulation method for flows with suspended paramagnetic particles has been developed. The method takes into account both hydrodynamic and magnetic interactions in a fully coupled manner. The magnetic forces acting on the particles are implemented via the Maxwell stress tensor. For the 2D problems investigated, the rigid-ring description turns out to be valid in the presence of actuation of the particles, but requires two times more collocation points on the particle boundary compared with the original description by Hwang et al. [21] where there is no actuation. The numerical scheme was verified with the problem of a single suspended particle in a stationary magnetic field generated by a current-carrying wire. Compared with results from a boundary-fitted mesh problem as a reference, the present scheme shows convergence to the reference solutions with mesh refinement. We have solved two problems containing more than one particle to demonstrate the feasibility of applying the method developed to practically relevant problems. In the first problem, two interacting magnetic particles move in a uniform field. We find the critical angle between the field and the line connecting the two particles to be approximately 45° in the case of two-dimensional circular particles, which determines the nature of interaction force to be either attractive or repulsive. The second problem concerns the motion of a chain formed by multiple particles, under the influence of a rotating field. The nature of deformation of the chain is dependent on the Mason number, the ratio of the

viscous force to the magnetic force. Chain break-up occurs within a certain range of Mason numbers. The deformation of the chain at break-up shows good agreement with previous work, deforming to a reverse S-like structure just before break-up and splitting into two chains. Since this scheme is a general direct method it can be extended to complicated magnetically non-linear materials, computationally intensive problems in three dimensions, and to viscoelastic fluids with suspended magnetic particles.

References

[1] R.G. Larson, The Structure and Rheology of Complex Fluids, Oxford University Press, New York, 1999.
[2] F.D. Goncalves, J.-H. Koo, M. Ahmadia, A review of the state of the art in magnetorheological fluid technologies Part I: MR fluid and MR fluid models, Shock Vib. Digest 38 (3) (2006) 203–219.
[3] A. Manz, N. Graber, H.M. Widmer, Miniaturized total chemical analysis systems: a novel concept for chemical sensing, Sens. Actuat. B: Chem. 1 (1–6) (1990) 244–248.
[4] M.A.M. Gijs, Magnetic bead handling on-chip: new opportunities for analytical applications, Microfluid Nanofluid 1 (1) (2004) 22–40.
[5] N. Pamme, Magnetism and microfluidics, Lab. Chip. 6 (1) (2006) 24–38.
[6] A. Rida, M.A.M. Gijs, Manipulation of self-assembled structures of magnetic beads for microfluidic mixing and assaying, Anal. Chem. 76 (21) (2004) 6239–6246.
[7] N. Pamme, A. Manz, On-chip free-flow magnetophoresis: continuous flow separation of magnetic particles and agglomerates, Anal. Chem. 76 (24) (2004) 7250–7256.
[8] H. Suzuki, C.-M. Ho, N. Kasagi, A chaotic mixer for magnetic bead-based micro cell sorter, J. Microelectromech. Syst. 13 (5) (2004) 779–790.
[9] R. Calhoun, A. Yadav, P. Phelan, A. Vuppu, A. Garciab, M. Hayes, Paramagnetic particles and mixing in micro-scale flows, Lab. Chip. 6 (2006) 247–257.
[10] M.A. Hayes, N.P. Polson, A.A. Garcia, Active control of dynamic supraparticle structures in microchannels, Langmuir 17 (9) (2001) 2866–2871.
[11] S. Melle, J.E. Martin, Chain model of a magnetorheological suspension in a rotating field, J. Chem. Phys. 118 (21) (2003) 9875–9881.
[12] S. Melle, O.G. Calderon, M.A. Rubio, G.G. Fuller, Microstructure evolution in magnetorheological suspensions governed by Mason number, Phys. Rev. E 68 (2003) 041503.
[13] M.A. Hulsen, TFEM Users Guide, Eindhoven University of Technology, Eindhoven, The Netherlands, 2006.
[14] R. Glowinski, T.W. Pan, T.I. Hesla, D.D. Joseph, A distributed Lagrange multiplier/fictitious domain method for particulate flows, Int. J. Multiphase Flow 25 (5) (1999) 755–794.
[15] J.A. Stratton, Electromagnetic Theory, McGraw-Hill Book Company, Inc., New York, 1941.
[16] R.E. Rosensweig, Ferrohydrodynamics, Dover Publications, Inc., Mineola, New York, 1997.
[17] T.B. Jones, Electromechanics of Particles, Cambridge University Press, New York, 1995.
[18] X. Wang, X.-B. Wang, P.R.C. Gascoyne, General expressions for dielectrophoretic force and electrorotational torque derived using the Maxwell stress tensor method, J. Electrostat. 39 (1997) 277–295.
[19] J. Jin, The Finite Element Method in Electromagnetics, John Wiley & Sons, Inc., New York, 2002.
[20] S. Osher, S. Fedkiw, Level Set Methods and Dynamic Implicit Surfaces, Springer-Verlag, New York, 2003.
[21] W.R. Hwang, M.A. Hulsen, H.E.H. Meijer, Direct simulation of particle suspensions in sliding bi-periodic frames, J. Comput. Phys. 194 (2) (2004) 742–772.
[22] HSL. A collection of Fortran codes for large scale scientific computation. http://www.numerical.rl.ac.uk/hsl, 2002.